Diwata-2: Earth Observation Microsatellite with a Compact Bus System, Electronically Tunable Multi-spectral Imager, and Amateur Radio Communications Capability

Ariston Gonzalez, John Leur Labrador, Delburg Mitchao, Marc Caesar Talampas, Joel Joseph Marciano Jr.
Electrical and Electronics Engineering Institute, University of the Philippines - Diliman
UP-Diliman, Quezon City, Philippines; +639991155006
ariston.gonzalez@eee.upd.edu.ph

Yuji Sakamoto
Department of Aerospace Engineering, Tohoku University
Aobayama Campus Research Complex, Tohoku University, Aoba-ku, Sendai City, Japan
sakamoto@astro.mech.tohoku.ac.jp

ABSTRACT

The microsatellite Diwata-2 was launched into the 600-km Sun-Synchronous Orbit (SSO) last October 29, 2018. It has a low-power, low-complexity, compact bus structure, capable of Earth observation and remote sensing mission through a 5-meter resolution Near-Infrared (NIR) High Precision Telescope (HPT) and a 125-meter resolution Space-borne Multispectral Imager (SMI) with two Liquid Crystal Tunable Filters (LCTF). The LCTF operates as an electronic-based band reconfiguration filter allowing for more than 600-channels of wavelength variation. As a secondary mission, Diwata-2 has full-duplex FM voice communications capability via an on-board module utilizing the amateur radio band at a 5W power requirement from mobile ground users.

The structure has a 500-mm cubic external dimension, with JAXA's Payload Attached Fairing (PAF) rocket interface and deployment mechanism. Deployable solar array panels (DSAP) were also introduced to increase the power generation capabilities of the microsatellite.

The importance of detailed structural-mechanical models for finite-element analysis allowed for accurate structural simulation results. The observed accuracy is within 5-Hz for the first two modes compared to the actual vibration test results. Lastly, strict management of in-flight procedures allowed for consistent satellite performance, while modification of satellite maneuver based on imaging observation results improved target pointing accuracy to within 5-km.

INTRODUCTION TO THE PHL-MICROSAT PROGRAM AND DIWATA-2

The Philippines is a resource-rich but calamity-prone country. It ranked third in the 2018 World Risk Index of most disaster-prone countries in the world with a value index of 25.14% [1]. Every year, the country is visited by an average of 20 typhoons every year, five of which are destructive [2]. Its location on the Pacific Ring of Fire also makes the Philippines extremely vulnerable to natural disasters like earthquakes and volcanic hazards [3]. Between 2000 and 2016, natural disasters caused over 23,000 deaths and affected roughly 125 million people. The associated socio-economic damage amounted to $20 billion with average annual damages of $1.2 billion [4].

Over the past few decades, Space technology and Geographic Information Systems (GIS) applications have become an indispensable part of the modern information society. As disasters become more and more frequent and intense due to the effects of climate change, the demand for these technologies is increasing. Space technology and remote sensing as a tool for comprehensive hazard and risk assessments, response, relief, and disaster impact assessment. Space-based information and products can also be used in other areas such as assessment of crop area extent, management of water resources, yield assessment studies, land suitability assessment for agriculture, precision agriculture, and urban planning.

To build resilience and improve evidence-based decision-making, the Philippine government through the state's Department of Science and Technology (DOST) innovation council, funded the PHL-Microsat Program whose aim is to build, launch, and effectively utilize micro-satellite technology for multispectral, high precision Earth observation. Apart from orbiting satellites, the program intends to build people and

infrastructure on the ground to support research, development, innovation, and academic activities relevant to space technology and applications. The PHL-Microsat program is a multi-agency research and development effort of the University of the Philippines-Diliman, Advanced Science and Technology Institute, Tohoku University, Hokkaido University, and Kyushu Institute of Technology.

The Diwata-2 Earth observation microsatellite is the successor and incremental update to the Diwata-1 microsatellite, Philippine's microsatellite released from the International Space Station's KIBO Japanese Experimental Module (JEM) last April 2016. The Diwata-2, a 500-mm cubic microsatellite, was launched into orbit via H-IIA rocket F#40 from the Tanegashima Space Center in Japan, last October 2018. Diwata-2 was built with flight-proven instruments from its heritage predecessor satellites RISING-2 and Diwata-1, while incorporating some proof-of-concept designs such as the Deployable Solar Array Paddles (DSAP), experimental attitude modules, and the Amateur Radio Unit (ARU).

Having the advantage of a more regular revisit via a sun-synchronous orbit, Diwata-2 was expected to capture images of the Philippines with a consistent angle of sunlight on the surface of the Earth. This allows images to be archived as reference data, which can be used in analysis and determination of damage extent from disasters, monitoring of heritage sites, assessment of changes in vegetation, cloud pattern observation and weather disturbance studies.

Meanwhile, experimental attitude modules, namely, experimental Attitude Calculation Unit (ACU-Ex) and Sun Aspect Sensor in Zenith (SAS-Z) were also added to the satellite. These are experimental units aiming to move up the Technological Readiness Level (TRL) by performing in an actual space environment. Ultimately, however, these units aim to complement the existing attitude determination and control system (ADCS) of the satellite.

Finally, an amateur radio payload was included to provide full-duplex frequency modulated voice communication via the public VHF and UHF amateur radio band. This payload serves as an emergency relay point for situations where terrestrial communication ground stations are inhibited by natural or man-made disturbances.

DIWATA-2 DEVELOPMENT & MISSION EXECUTION OVERVIEW

The development of the Diwata-2 microsatellite follows the *"mission first"* philosophy in which the spacecraft design considerations primarily support the requirements of the project mission and objectives. The start of the development phase will go through an Engineering Model (EM) variant where modules and subsystems were developed with testing, validation, calibration, and iteration steps in place. In this phase, the prototype bus and payload instruments are integrated into software-in-the-loop and hardware-in-the-loop configurations for conformity and cross-module functional evaluation. To assess the qualification and acceptability level of the microsatellite design, space environment tests are conducted on the EM variant, both on the unit level and on system level. Even in the Diwata-2 EM development phase, several options were still being considered for the orbital launch provider. This led to several EM iterations of Diwata-2, mostly attuned to qualify for an ISS release or for a direct to space launch. The final configuration of the EM subsystems will also become the ground variant microsatellite system, serving as a verification and experimentation platform. This is useful for cases such as verification of command routines and maneuvers prior to in-orbit implementation.

After major testing of the EM variant and finalization of the orbital launch provider, a qualified and validated design provides the basis to start the development of the microsatellite Flight Model (FM) variant. In this phase, the fabrication of the FM components for the Bus and the mission payload instruments are conducted. The final flight configuration, as validated from the EM tests, of the hardware and software aspects of the system are integrated as the microsatellite FM. The flight model is subjected to the specific launch environment (shock test, random vibration test, rocket interface conformance checks, deployment switch test) and the space environment (thermal-vacuum test, communications, and functionality test). The verification of the test results will provide the basis for the qualification and acceptability of the microsatellite for launch into space.

Post-launch, during the initial phases of the space flight, procedural and systematic commissioning of the microsatellite commences. This allows for safe and controlled verification of in-flight performance. Important aspects to consider are the predictable conformance of the general microsatellite health status to preflight ground results. Necessary calibration and

system tweaks are also implemented at this phase, to achieve ideal performance. The development and mission execution workflow of Diwata-2 is shown in Figure 1.

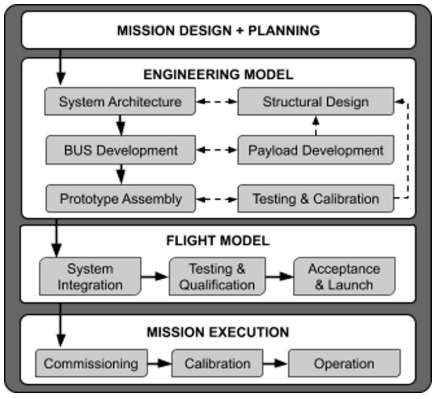

Figure 1: PHL-Microsat's Small Satellite Development Workflow

DIWATA-2 BUS OUTLINE

The microsatellite bus serves as the supporting system for the realization of the mission objectives. Diwata-2's bus system derives heritage from its predecessor Diwata-1 and Rising-2 [8][9]. Key modifications on the power supply subsystem, and performance improvements on the other subsystems, can be found in Diwata-2. The additional capability to host experimental engineering modules under the Attitude Determination & Control Subsystem (ADCS) is also included.

System Architecture

The system architecture of Diwata-2 was designed to achieve an Earth observation mission with optical payloads, requiring attitude re-orientation, targeted pointing maneuvers, high-speed data downlink, and system power management. The system block diagram of the Diwata-2 subsystems is shown in Figure 2.

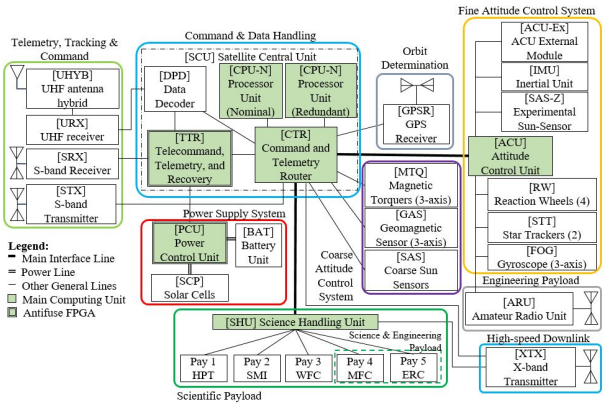

Figure 2: Diwata-2 System Diagram

Structural Design of the Bus

The structural design considerations for Diwata-2 relied heavily on the constraints of the target orbital launch provider, Mitsubishi Heavy Industry's H-IIA rocket. Diwata-2 was designated as a piggyback secondary small satellite payload on the rocket's satellite fairing stage. The satellite attachment interface and deployment mechanism from the rocket was the JAXA proprietary Payload Attach Fitting (PAF) rocket interface with clamp band [5]. Important constraints associated with the rocket launch that needs to be considered in the design are the following:

- The main structural envelope of the microsatellite must be within 500mm x 500mm x 500mm.
- The center-of-gravity offset must be within 250mm and 25mm in the longitudinal and orthogonal direction, respectively.
- Moment of inertia in each axis must be within 1kg-m^2.
- The fundamental frequency of 100Hz or less in the longitudinal direction and 50Hz in the lateral direction.

The structural configuration of Diwata-2 was based on a central pillar back-bone that supports the majority of the bus components' mass. This design configuration is closely similar to the previous designs from Tohoku University satellites such as *SpriteSat* and *RISING-2*. Despite the similarities in terms of rocket launch and orbit, slight changes in the design were introduced. The central pillar was interconnected to all side panels. This resulted in a stronger and more rigid structure and allowed more room for other payloads and a larger clearance for all the cameras' field of view (FOV).

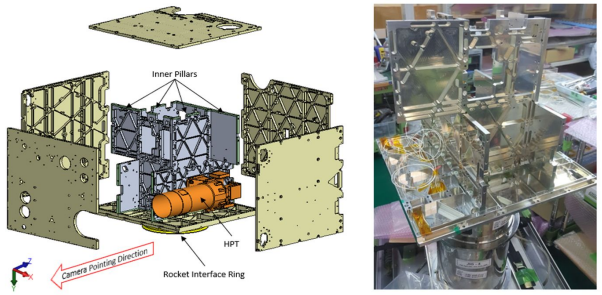

Figure 3: Internal Structure of Diwata-2 Showing the Central Pillar Configuration

To reduce the overall structure mass and achieve a more optimal mass-to-strength ratio, isogrid stiffening pattern was applied to all panels made of aluminum alloy material.

Another design improvement was the addition of a deployable solar array paddle (DSAP). The DSAP can be divided into four major parts: paddle, hinge mechanism, lock mechanism, and release mechanism. Initially, during launch, it is held down by Dyneema wires. Once ground operators send the command to deploy these panels, the burning mechanism is activated cutting the wires holding down the DSAP. The design utilized materials such as aluminum alloy 6061-T6, stainless steel, carbon fiber reinforced plastic (CFRP), and a thermoplastic polymer called polyether ether ketone (PEEK).

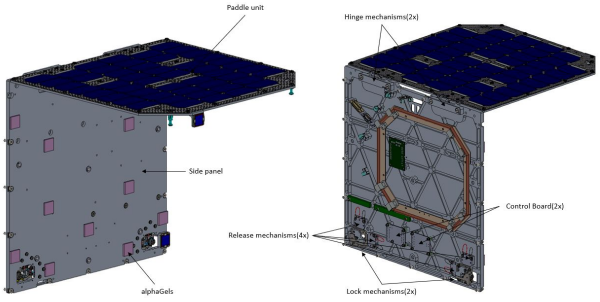

Figure 4: CAD Model of Diwata-2's Deployable Solar Array Paddles

To eliminate unnecessary guesswork and derive accurate dimensioning of wire lengths, multiple electrical cable route subassemblies connecting each component were created using *SolidWorks*® add-in feature called Routing Application.

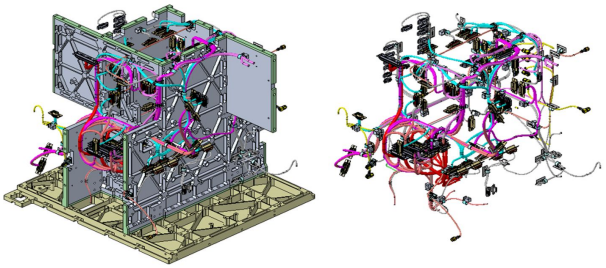

Figure 5: Wiring Harness Routing in Diwata-2

In order to verify the integrity of the bus structure developed before fabrication, a finite-element model of the bus was developed in FEMAP® with NX Nastran, an analysis structure simulation software. The 3D CAD model with isogrid milling was imported to the software. The simulation model consists of hex meshes with a total of 29,741 elements, and 68,182 nodes. Payloads were modeled as mass points and actual bolt connections were assumed as glued connections with an estimated "bonding force" based on the bolt type. Normal modes, quasi-static, and random vibration analyses were performed using the meshed model in Figure 6.

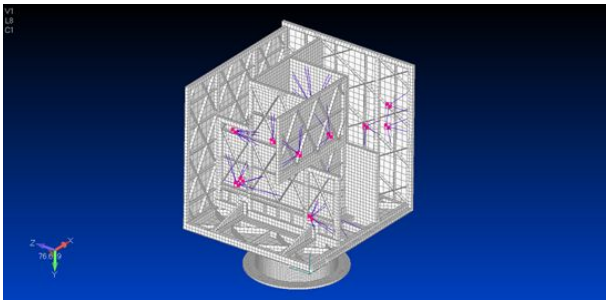

Figure 6: FEMAP® Model of Diwata-2 with Isogrid Patterns

The structure design met the launch vehicle's main critical criterias of a first natural frequency that is greater than 50Hz and margin of safety in measured stress that is greater than zero. These are verified through the FEMAP® software.

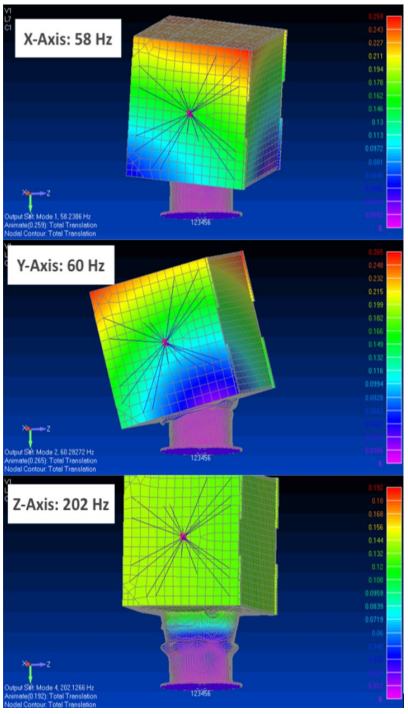

Figure 7: First Normal Mode Visualization on each of the Three Orthogonal Axes

Table 1: Miles Equation Calculation (Factor of 3)

Vibration Axis	First Eigenvalue (Hz)	GRMS	Max Von Mises Stress (Mpa)
X-Axis	58.24	16.23	178.3
Y-Axis	202.12	30.24	136.82
Z-Axis	60.28	16.51	163.77

The margin of safety values calculated for yield and ultimate stress were 0.75 and 0.78, respectively, using Equation 1. The calculation showed that the structural design was acceptable and met the criteria set by the launch provider.

$$MoS = \frac{F}{\sigma \times FF} - 1 \quad (1)$$

where F = material yield/ultimate strength; σ = maximum von Mises stress; and FF = fitting factor (Yield = 1.25; Ultimate = 1.5).

Thermal Design of the Bus

In conjunction with the structural analysis, the thermal design was performed. With the challenges posed by real-time active temperature control of critical components, the thermal conditions of Diwata-2 were passively managed instead. Passive control was implemented through conductive isolation of the outer panels from the inside panels using glass epoxy. This mitigates large temperature variations on the internal components. In addition, the surfaces of side panels were covered with Kapton polyimide tapes. Unlike paints which are permanent, final absorptivity and emissivity of each panel may still be adjusted by modifying the total area of Kapton polyimide in each panel.

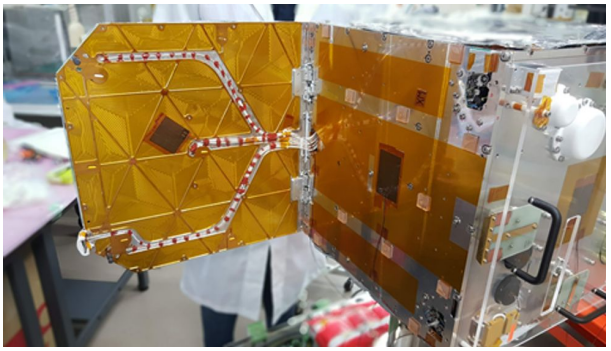

Figure 8: Diwata-2 covered with Kapton Polyimide Tapes

Simulations were carried out using Thermal Desktop® with SINDA/FLUINT and RADCAD, a complete CAD-based thermal engineering tool suite. A thermal mathematical model with multiple nodes was created. The model was set in a sun-synchronous orbit at an altitude of 600-km with a local time of descending node (LTDN) around 11:00 am. Worst hot and cold case conditions of the satellite in-orbit considered were as follows: Stowed and Nadir, Deployed and Nadir, Deployed and Sun-pointing.spacecraft is oriented so that the solar panels are always facing the sun. The thermal model was run for around 970 minutes (~10 orbits) with one-minute time steps for all cases. Temperatures in Kelvin at each time step in the 10th orbit were exported for validation and comparison purposes. The area covered by Kapton polyimide was adjusted until the temperature range of 0 to 40℃ for components, -20 to 60℃ for external panels, and -40 to 70℃ for DSAP were satisfied.

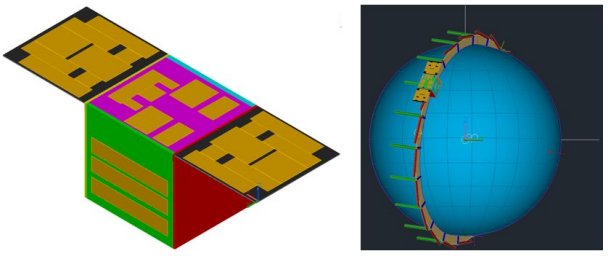

Figure 9: (L) Thermal Mathematical Model created in Thermal Desktop® (R) Sample Orbit Representation of a Test Case

Telemetry, Command, and Data Handling Subsystem

At the core of the satellite's command parsing, telemetry handling, and data management is the Satellite Central Unit (SCU). To achieve high-reliability and long-term flight performance, the SCU has a redundant processing unit, and a Telecommand, Telemetry, and Recovery (TTR) processing block which are all built on a reprogrammable flash FPGA. Techniques in fault tolerance, isolation, and recovery within the SCU were implemented due to its critical role in the satellite operation.

The mission data is managed by the SCU from the relevant mission modules and is also in charge of relaying the combined telemetry and housekeeping information of the satellite modules.

Power Subsystem

The satellite generates power through the solar cells pasted on the surface of the majority of external panels. The produced power is then stored in a Nickel-Metal Hydride (Ni-MH)-based battery unit. Meanwhile, a power controller in the form of the Power Control Unit (PCU) manages charge and discharge activities among the battery, solar cells, and bus modules acting as load elements.

Ultra Triple Junction (UTJ) solar cells with an efficiency of 28.3% were used in Diwata-2. Each cell can generate an average of 1 W over its 26.62 cm^2 area. A total of 170 cells configured as 17 strings of 10 cells each were positioned to cancel out magnetic fields induced by current loops from the solar cell strings.

Diwata-2 had a total of 18 Ni-MH batteries configured in a 9-series by 2-parallel configuration. This configuration allowed redundancy as only one of the parallel storage is used at a time. Each cell is rated at 1.2 V and 3700 mAh, which gives the entire battery unit a nominal voltage of 10.8 V and 7400 mAh capacity. The battery cells used in the battery unit are the 18 average-performing cells out of an initial pool of 100 industrial-grade commercial-off-the-shelf variants that were subjected to thermal and vacuum tests. The selected cells were finally packed in a vibration-resistant and thermally-controlled (black anodized) enclosure.

Meanwhile, the PCU acts as the charge and discharge controller of the satellite. It ensures that the satellite bus components receive a stable power supply at any phase in orbit. The PCU also monitors, and more importantly, recovers the satellite from the following conditions:

1. Battery overcharge
2. Battery under-charge
3. Load short-circuit
4. High battery temperature

To ensure the high-reliability of the PCU, a radiation-hardened one-time-programmable (OTP) antifuse field-programmable gate array (FPGA) was used for the logic part.

Upon releasing the deployable solar array paddles (DSAP) from its stowed position, power generation capacity can be significantly increased by maneuvering the attitude of the microsatellite into a sun-tracking mode. In this mode, maximum power point tracking of the 130 solar cells of the DSAP and the positive zenith external panel cells is achieved by active re-orientation towards the solar direction.

The DSAP increases the power generation potential of the satellite from an average of 38.72W during free rotation mode in the sunshine, to 132.6W after DSAP deployment and sun-tracking attitude mode. With power consumption ranging from 40W to 58W during operation (11% of the orbit) and 11W at standby (89% of the orbit), around 17% power budget is achieved with nominal power generation.

The satellite's typical operation modes are generally categorized into a standby mode with telemetry-command data handling communications, a mission observation mode with active attitude control, and a high-speed communications mode with attitude control. The standby with telemetry-command data handling mode consumes around 10.8-W. This mode involves the constant power activity of the PCU, SCU, GAS, GPSR, and the important housekeeping telemetry and command communication modules on the S-band and UHF-band. From the standby mode, active attitude control can be achieved by activating the ACU, FOG, STT, and the reaction wheels. Active attitude control mode typically consumes 39.5 W during peak rotation of the reaction wheels at 2000 RPM. For the mission observation modes, the activation of the SHU and the mission instruments are paired with active attitude control for target pointing and maintaining satellite stability. The specific power consumption would depend on the combination of mission instruments that are activated, ranging from 47 - 53.3 W. The observation mode peak consumption involves all the payload: WFC, MFC, ERC, SMI, and HPT. Lastly, the

high-speed communications mode simply utilizes the dedicated X-band module for high data rate transmissions. In this mode active attitude control is used to maintain the strongest link between Diwata-2 and the ground station. Table 2 shows the characterized power budget of Diwata-2 under the combination of these typical operation modes.

Table 2. Power Budget of Diwata-2 Satellite.

Mode	Standby with Telemetry / Command	Observation with Attitude Control	High-speed Download with Attitude Control
Power Consumption	10.8 W	47 - 53.3 W	60.10 W
Discharging Current	0.99 A	4.352 - 4.935 A	5.564 A
Duration	22 hrs/day	1 hr/day	1 hr/day
Discharging Capability (DC)	21,780 mAh/day	4,352 - 4,935 mAh/day	5,564 mAh/day
Peak Net DC	32,279 mAh/day		
Total # of solar cells			170
Avg. number of cells exposed to sun			42.93
Avg. generated power of solar cells @ 80℃			38.72 W
Charging capability (Stowed DSAP)			46,269 mAh/day

Even without deploying the DSAP, the net power discharge of Diwata-2 can be managed by allocating sufficient duration for standby modes over areas without target image acquisition. High-speed download mode is typically conducted over areas within ground station range only. For these general cases, a typical peak net discharge is expected around 32,279 mAh/day, which is conservative and well below the average charging capability of 46,269 mAh/day.

Communications Subsystem

Diwata-2 has several bands to establish communication links with the ground station segment. For commanding and telemetry, there is a communications link on the UHF band and the S-band. For high-speed data downloads, the X-band link is used.

Mission data uses both the S- and X-band downlink channels. The maximum speed for the S-band downlink is 100kbps. This corresponds to 56 seconds download time for an image with a size of 0.7MB, or 2 minutes and 40 seconds download time for attitude data with a size of 2MB. On the other hand, the maximum speed for the X-band downlink is 2.4Mbps. An image with a size of 0.7MB can be downloaded within 2.3 seconds using this band.

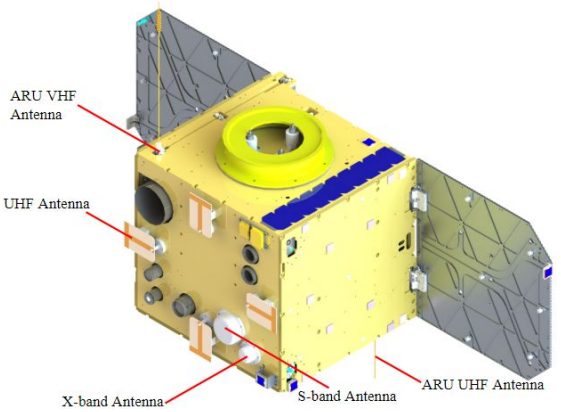

Figure 10: Antenna Locations in Diwata-2

Attitude Determination and Control Subsystem

The microsatellite's ADCS generally consists of the attitude sensing subsystem, the attitude re-orientation/actuation subsystem, and the attitude calculation and management unit. For the attitude sensing subsystem, there are two general attitude determination modes: the coarse attitude determination and the fine attitude determination. Under the coarse attitude determination, the Geomagnetic Aspect Sensor (GAS) and the Sun Aspect Sensor (SAS) are used. Meanwhile, for the fine attitude determination, two Star Tracking Telescope (STT) modules are utilized. For any determination mode, the Global Positioning Satellite Receiver Module (GPSR) is operated for satellite position and velocity confirmation in tandem with the onboard SGP4 orbit calculation. In addition, a Fiber-Optic Gyroscope (FOG) module is used to determine the satellite's rotational speed, which can consequently be used to propagate an initially determined satellite orientation even without new information from the coarse or fine sensors.

The main on-board computer conducting the attitude sensor handling, attitude determination, and attitude control of the microsatellite is the FPGA-based Attitude Computing Unit (ACU). The ACU conducts IGRF based Earth magnetic field modeling, solar position

modeling, SGP4 based satellite position and velocity calculations, ADCS related command handling, sensor measurement handling, alignment calibration management, satellite attitude estimation, and the overall satellite attitude control through the relevant actuators.

To conduct satellite re-orientation maneuvers, the satellite has two attitude actuator modules: the Magnetorquer Units (MTQ) for coarse control, and the Reaction wheel Units (RW) for fine control. There are three MTQs, one for each rotational axis, and four RWs systematically oriented to maneuver on all rotational axes. The magnetorquer units are generally used to stabilize the satellite from a tumbling state and reduce the angular speed to less than 3-degrees per second. The MTQ has the performance ability to decrease the rotation speed down to 0.06-degrees per second, same as the orbital angular velocity of the nadir pointing frame. But around 0.5-degrees per second is maintained for the standby free-rotation to ensure that solar heat over time is distributed across multiple areas of the satellite. To accurately point the satellite to a more specific target, the three-axis reaction wheel system is used to finely maneuver and rotate the satellite; consequently re-orienting the mission instruments.

Diwata-2 general attitude maneuvers include nadir pointing mode, single-target tracking mode, point-to-point target tracking, fixed quaternion/inertial based orientation, and manual off-nadir orientation maneuvers.

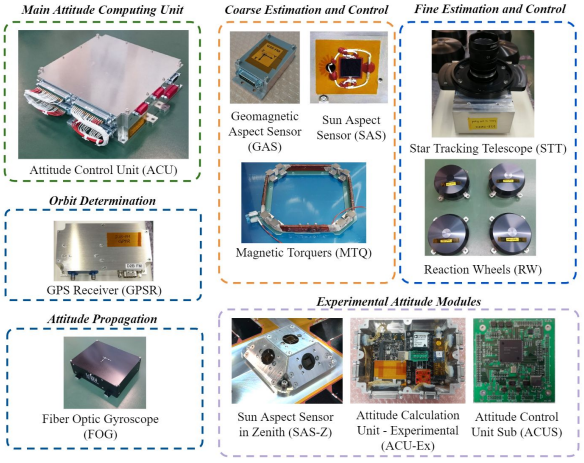

Figure 11: Diwata-2 ADCS Modules

Additionally, experimental modules for compact, cost-efficient attitude estimation were also included in the Diwata-2 ADCS. The Sun Aspect Sensor in Zenith (SAS-Z) is an experimental module for solar position measurement, wherein multiple quadrant photodiode based sensors were used in a trapezoidal prism configuration for minimal and manageable inter-sensor misalignment. The SAS-Z has an FPGA-based on-board computer for conducting the solar position estimate based on the light-sensitive sensors' values, and for handling misalignment calibration parameters. A complementing experimental Attitude Calculation Unit (ACU-Ex) was also integrated, containing a commercial-off-the-shelf inertial sensor, magnetic field sensor, and an ARM-based computer. The ACU-Ex by default conducts standard functionalities of solar position modeling, magnetic field modeling, and calculates attitude estimation based on the SAS-Z solar position values, and the magnetic field measurements. Experimental approaches to attitude estimation using onboard statistical filtering and data regression were also implemented on the ACU-Ex as estimation mode options.

Lastly, a separate experimental Attitude Control Unit Sub (ACUS) has also been included for higher-order environmental model calculations [12].

DIWATA-2 MISSION & PAYLOAD OUTLINE

Earth Observation and Remote Sensing

Several scientific optical instruments were integrated into the microsatellite bus. The primary payloads managed for remote sensing are the High-precision Telescope (HPT) and the Space-borne Multispectral Imager (SMI) camera with Liquid-Crystal Tunable Filters (LCTF) [7]. The HPT uses a Cassegrain-based optical design with four separate CCD imaging sensors, one for each of the NIR/R/G/B bands [10]. At the 600-km orbit altitude, it has an overall field-of-view of 3.1 x 2.3 km and a spatial resolution of 4.7-m. The multi-spectral camera SMI has two LCTF, one dedicated for the 433-740nm bands, and another on the 730-1020nm bands. This is the primary workhorse for doing remote sensing work, with the capability to change the wavelength within 39-259 milliseconds across 400 bands within a 5.1-22.1 nm bandwidth. The SMI's field-of-view is 83.7x62.7-km and a spatial resolution of 126.9-m.

Supporting scientific payloads include the Enhanced Resolution Camera (ERC), the Wide-field Camera (WFC), and the Middle-field Camera (MFC). The ERC is a CCD based panchromatic camera used for pansharpening the SMI images. It has a field-of-view of 89.8 x 67.5 km and a spatial resolution of 54.6-m. The MFC is another CCD based camera, primarily used for geolocation assistance of the HPT and SMI images. It

mainly takes RGB colored images, has a 189.3 x 141.9 km field-of-view, and a spatial resolution of 287.2-km.

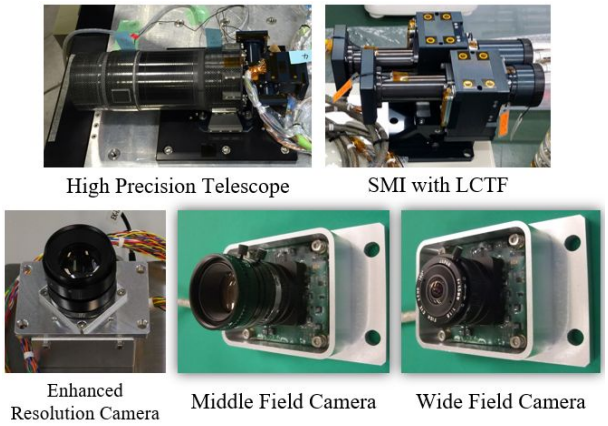

Figure 12: Flight Model of Optical Payloads

Lastly, a separate on-board computer called the Science Handling Unit (SHU) manages the command and data handling of the mission instruments. Non-volatile memory submodules on the SHU are used as the primary storage of the mission data.

Emergency Communications

To achieve emergency communications capability, Diwata-2 was equipped with the custom Amateur Radio Unit (ARU), containing a Frequency-Modulated Voice Repeater (FMVR) sub-module and an Automatic Packet Reporting System (APRS) based message broadcasting capability, all operating on the amateur band frequencies. With this payload, Diwata-2 was officially designated as an Orbiting Satellite Carrying Amateur Radio (OSCAR) with the callsign *DW4TA-1*.

The ARU used the 145.9 MHz amateur band frequency for its APRS/VR/Beacon downlink signals, and the 437.5 MHz frequency for the APRS/VR uplink signals. The FMVR capability was used as the bridge for bi-directional analog voice communication, built around a single radio receiver sub-module, and a single radio transmitter sub-module. The transmitter sub-module also provided a continuous wave Morse code beaconing function for broadcasting the ARU housekeeping telemetry. A *Bell-202* compliant modem was used in conjunction with the transceiver modules to achieve APRS-based data messaging capability. The module's main computing board was based on the *Vorago VA10820 REB1* development board, taking advantage of the relatively cost-efficient and radiation-hardened *VA10820* ARM-based microcontroller chipset.

Figure 13: ARU Computer and Radio Transceiver Module

The communication antennas for the ARU were two quarter-wave monopole design antennas with custom deployment mechanisms. One monopole antenna is designed for the 144-146 MHz segment of the Very High Frequency (VHF) band, and another monopole antenna for the 435-438 MHz segment of the Ultra High Frequency (UHF) band. Monopole antennas were selected for their omnidirectional radiation pattern and for the simplicity of the design and deployment considerations [11].

Table 3: Specification of the Amateur Radio Antenna and Deployment Mechanism

Parameter	Target
Type	Quarter wave monopole
Frequency Range (FR)	144 MHz-146 MHz (VHF ANT); 435 MHz-438 MHz (UHF ANT);
Radiation Pattern	As omnidirectional as possible (>0 dB gain in a wide range of directions)
Polarization	Linear
Reflection coefficient	<-10 dB within FR (VSWR of 2:1 or better)
Impedance	50 Ω
Materials	Aluminum (antenna rod), PEEK (movable hinge), Al (fixed hinge), stainless steel (spring and screws) and FR-4 PCB
Deployment and Release Mechanism	Torsion-spring loaded hinges; Stowed position: antenna rod tied to a Dyneema rope using a burnt resistor

The ARU module can be activated via ground commands to Diwata-2 through its official command and data handling parameters, but not via the amateur

band link. The antenna deployment utilized a rope tightened latch-lock system that gets released via nichrome wire heating to cut the *Dyneema* based ropes. This wire-cutting mechanism is triggered automatically as a scheduled sequence upon the initial activation of the ARU module.

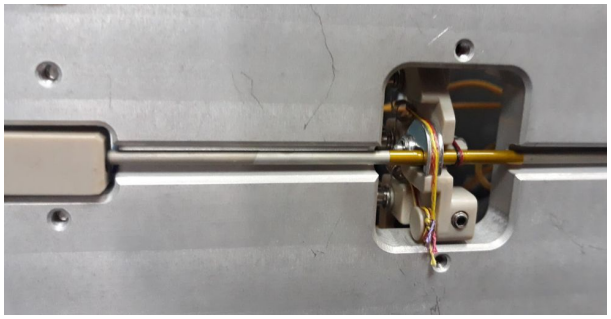

Figure 14: Stowed ARU UHF Antenna with Custom Deployment Mechanism

DIWATA-2 PRE-FLIGHT TESTS & EVALUATION

Electronic Functionality Testing

To ensure a verified and predictable manner of operations, a systematic electronic functionality test of the microsatellite was conducted on the ground during multiple phases of the development. These tests allow for interface conformity, detection of functional errors, performance characterization, calibration routines, and detection of other possible performance anomalies. There are two general strategies for conducting the electronic functionality evaluations, a software-in-the-loop (SIL) testing, and hardware-in-the-loop testing (HIL). In the SIL setup, portions of the Bus subsystem are replaced by simulated models from custom and proprietary software, emulating ideal condition values or systematically prepared error values. In Tohoku University, real-time simulation systems that model the space environment and the satellite dynamics are developed and implemented [16]. The satellite dynamic models and sensor measurement simulation are constantly improved through related theory and performance results of in-orbit microsatellites [17]. On a HIL setup, the bus subsystems under test are interfaced into physical equipment substitutes. During the FM electronic functionality tests, the EM variant of the modules is configured and used as a reference satellite testbed platform.

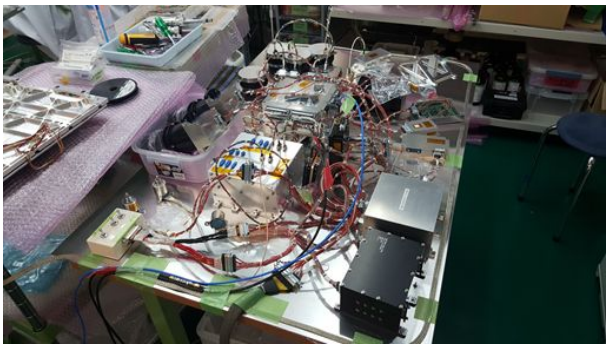

Figure 15: Diwata-2 Satellite Test Bed Platform

The electronic functionality tests of Diwata-2 were conducted as frequently as possible, notably prior and subsequent to the major space environment qualification tests. Early in the microsatellite development, initial functionality tests were formed and conducted as a benchmark for the microsatellite's performance. These tests cover performances in the categories of power, communications, C&DH, and various specific module metrics. These standardized procedures were conducted subsequently to major environment testing, ensuring that the microsatellite had a repeatable and consistent performance. Any deviations on the benchmark results were indicative of possible faults in the system and were subjected to closer scrutiny for corrective actions.

The final performance results of the Diwata-2 FM were also used as the baseline reference for the in-orbit performance of the microsatellite. These are used for regular operations and housekeeping monitoring.

Antenna Radiation Pattern Test

All communications hardware of Diwata-2 were subjected to radiation pattern tests to verify the directivity of the front-end link. These tests were conducted on an anechoic chamber to eliminate stray sources of radio signals and produce repeatable results. In this test, a source antenna produces the reference source signal, while the modules under test are placed on a rotating platform. The received signal levels are recorded.

Figure 16: Diwata-2 Antenna Radio Pattern Test

Thermal-Vacuum and Off-gas Tests

Earlier in the development phase, the engineering model was subjected to thermal balance tests. Whereas, the flight model of Diwata-2 underwent off-gas and thermal vacuum tests. All the tests utilized a vacuum chamber housed in the Space Mission Center (SMC) at Hokkaido University, Japan. The chamber has a shroud dimension of Φ1000×D1545-mm and operates at a vacuum pressure around $\geq 10^{-4}$ Pa. Kapton tape and ceramic heaters were used to introduce total heat the satellite may absorb in-orbit. These heaters are controlled by four 60V-6A and two 80V-4.5A variable-switching regulated DC power supplies. Thermal balance test results were used to improve the accuracy of the simulation model. Meanwhile, a thermal vacuum test was performed to verify the in-orbit performance of the satellite through functionality tests during worst-case conditions.

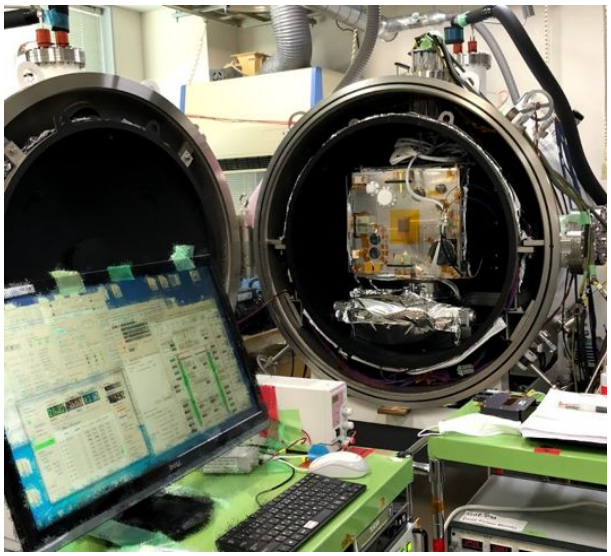

Figure 17: Thermal Vacuum Test Set-up of Diwata-2 Flight Model

Vibration Test

Critical testing required for launch qualification is vibration test. Diwata-2 underwent a total of 12 vibration tests covering sinusoidal and random vibration evaluations. The results of each vibration test significantly contributed to the design iteration of the satellite structure from a mechanical test model with dummy mass, to the EM variant, and finally to the FM variant. The vibration levels used for the FM were conformant to the HII-A rocket launch; Table 4 shows the random vibration parameters and Table 5 shows the sinusoidal vibration test level requirements.

Table 4: Random Vibration Test Level for the H-IIA Rocket Launch

Frequency Width (Hz)	**Acceleration** (G^2 / Hz)
20-200	+3 dB/octave
200-2000	0.032
Actual	7.8 Grms

Table 5: Sinusoidal Vibration Test Level for the H-IIA Rocket Launch

Direction	**Frequency** (Hz)	**Acceleration**
Longitudinal Direction	5-100	24.52 m/ s^2
Lateral Direction	0.032	19.62 m/ s^2

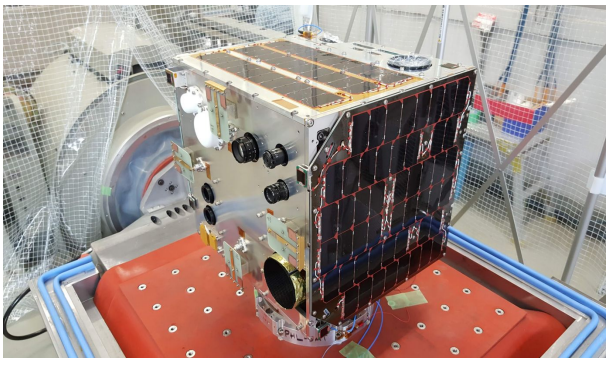

Figure 18: Vibration Testing at the Miyagi Industrial Technology Institute Facility

Shock Test

The separation procedure of Diwata-2 from the rocket depends on the controlled explosion of the attachment bolts on the PAF rocket interface. This procedure imparts shock on various points of the microsatellite, notably on the PAF attachment side where the

deployment switches are located. To ensure that the deployment switches are undamaged after the separation procedure, Diwata-2 was subjected to a shock test at JAXA's Tsukuba Facility. The microsatellite was suspended off the ground via crane hook attachments and dummy explosive devices were attached at the designated rocket attachment points. After the controlled pyrotechnic shock test, the microsatellite did not encounter any mechanical or electronic issues.

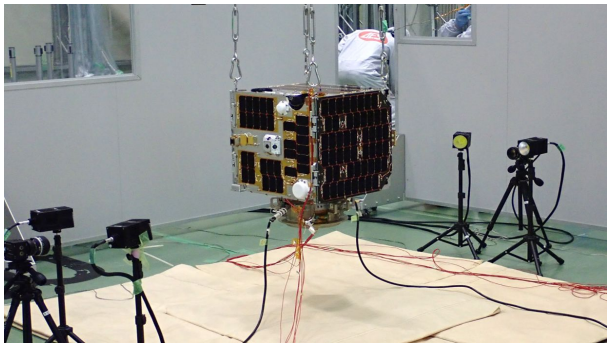

Figure 19: Separation Shock Test Setup at JAXA

DIWATA-2 IN-ORBIT EVALUATION AND OPERATION

After the qualification and acceptance of Diwata-2, the microsatellite was handed-off to JAXA with an official mass of 57.36-kg. The microsatellite was successfully launched into orbit on October 29, 2018 from the Tanegashima Space Center in Japan. Diwata-2 was attached to the small satellite piggyback fairing of MHI's H-IIA F#40 rocket along with the main payload GOSAT-2. The ground receiving stations in Manila, Philippines and in Sendai City, Japan were tasked with establishing contact with the satellite.

Bus Subsystems Flight Commissioning Evaluation

The first week of operations were dedicated to the verification of the bus system capabilities. A stable and reliable telemetry link was immediately confirmed with the satellite during its first pass over the Philippine ground station after the launch. The command link was also confirmed on the subsequent passes. To systematically and programmatically evaluate the satellite, a list of scheduled commands was prepared on the ground and uploaded to the satellite. The first phase of the trials was focused on evaluating the power consumption of each subsystem and its corresponding individual modules. Without any active attitude control, a peak Bus power of 24.26-W was observed after sequential activation of the ADCS subsystem modules: GAS, GPS, ACU, and Mission-related modules: SHU, WFC, MFC, and ERC. To safely evaluate the SHU, the initial mission instrument to be tested was the WFC. The WFC's wide field of view allowed for a greater chance of imaging recognizable LEO features, with minimal snapshot count, and even without active attitude control.

With stable module activations, attitude control trials through MTQ de-tumbling, RW rotations and speed were successfully evaluated. Subsequently, imaging using the mission instruments with active attitude control were also conducted.

Lastly, high-speed download using X-band and active target pointing towards the ground station maneuver was successfully conducted over several passes. The peak power registered from the telemetry for this mode was 56.05-W.

Experimental Module Evaluation

The experimental ACU-Ex and SAS-Z solar position sensor was successfully activated after the initial Bus subsystems commissioning phase. To maintain a relatively controlled testing condition, the microsatellite Diwata-2 was set to a nadir-pointing mode over the Philippines during times of data gathering. Since the orbit is sun-synchronous, the flight maneuvers over the Philippines are typically conducted within 12:00-13:00 UTC+8. Eight case studies from different flight passes of Diwata-2 have been considered.

On the April 4, 2019 flight data, it can be observed that there are significant discontinuities on the SAS sensor's solar vector measurement, represented by the ACU-X,Y,Z parameters on Figure 20. These discontinuities are hypothesized to occur due to the physical switching of one SAS to another. Between the multiple SAS sensors, there is an uncalibrated misalignment with respect to the other sensors, resulting in an incohesive transition between the individual sensors. With SAS-Z, the statistically derived misalignment correction factors between the different quadrant sensors have been used to provide a cohesive transition, represented by the SASz-X,Y,Z parameters on Figure 21.

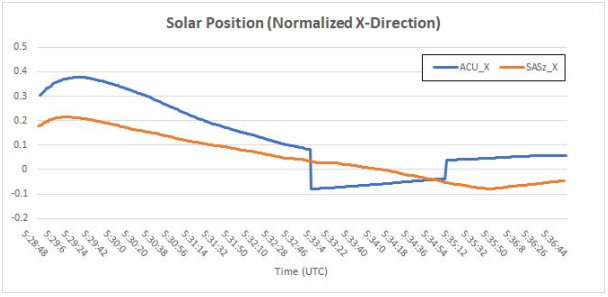

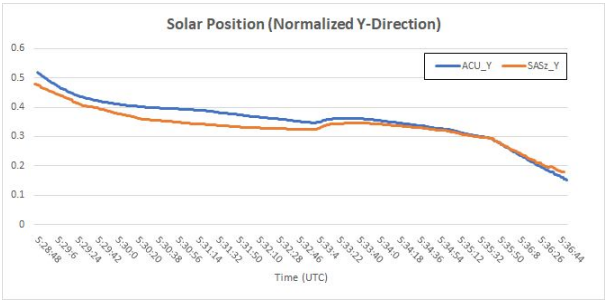

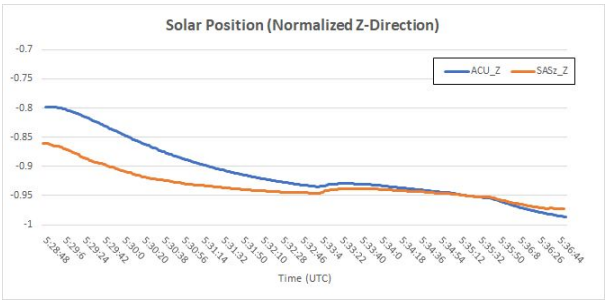

Figure 20: Solar Vector Measurement of Diwata-2 SAS and SAS-Z

Emergency Communications Operation

The ARU payload was activated after Diwata-2's first month in orbit. On its initial activation the UHF antenna for uplink was deployed. On the next day-pass over the ground station, the VHF antenna for downlink was also deployed.

The first beacon from the ARU payload was received on November 30, 2018, between 13:55:01 to 14:00:01 (GMT+8). The very first decodable beacon sent by the ARU payload was: ***MABUHAY PILIPINAS DW4TA 000000C0 0008 CCC1 2CC03C017.*** This contains an information of 192-secs of uptime, 8 reboots, deployed state for both VHF & UHF antennas, a module voltage of 11.51 V, a current draw of 0.2418 A, and a module temperature of 23 °C. The raw signal from the first beacon broadcast containing these telemetry information can be seen in Figure 21.

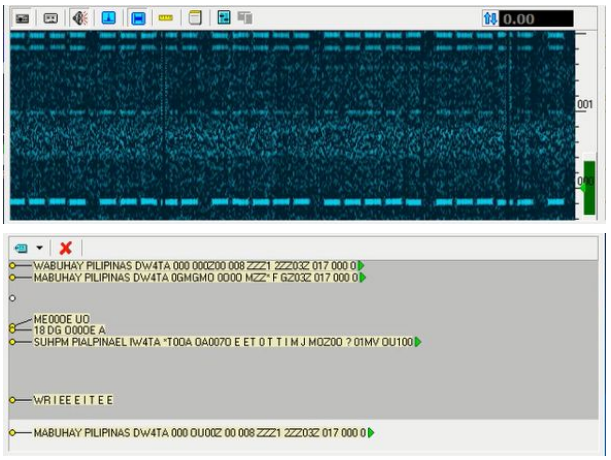

Figure 21: Signal snippet from the first beacon broadcasted by the ARU and decoded at the UP EEEI amateur ground station

Furthermore, the beacon data confirmed that the in-flight power consumption of the ARU corresponds to the ground evaluations, with peak power draw of 2.98-W during FMVR operations.

One of the farthest live duplex voice conversations via the ARU transpired on March 10, 2019, 13:31 (GMT+8), with a user from Laguna, Philippines communicating with another user from Okinawa, Japan.

Earth Observation Mission Operation

Launched at 621-km altitude, the sun-synchronous orbit of Diwata-2 allowed for an 11-day revisit period over a specific target area. Images can now be captured and analyzed to track the spatiotemporal changes of various geophysical variables. In a single pass, multiple consecutive images can be taken by each optical instrument effectively covering a wider area. Ground processing of the images can be done to stitch the images together and form an image mosaic. A stitched mosaic composed of 20 SMI and 20 ERC images of the Visayan islands in the Philippines are shown in Figure 22. These images were taken on December 14, 2018, 12:53:31 (GMT+8).

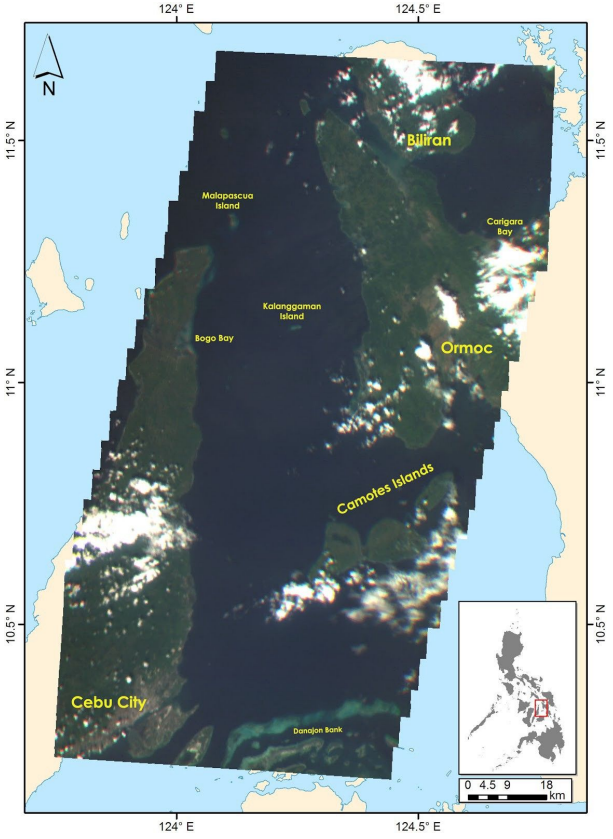

Figure 22: SMI+ERC Stitched Images

The ERC images were used to pansharpen the SMI images and bring the spatial resolution to 54.6-m. In Figure 23, a contrast between a raw SMI image from the mosaic is shown pansharpened with the accompanying ERC image.

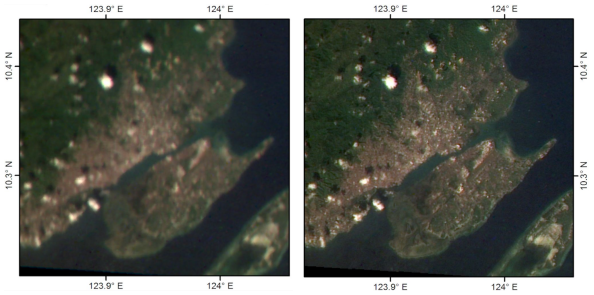

Figure 23: Pan-sharpened Image of SMI in conjunction with ERC.

The wider swath and higher signal-to-noise ratio of the imaging instruments of Diwata-2 allowed for in-depth studies of water quality, making it particularly useful for high-value coastal and inland water monitoring, From March 2019 to June 2019, images were taken over the Philippine's largest lake, the 900 km^2 Laguna Lake, for water turbidity analysis and spatial variability observations. Ground truth reference via in situ water sampling measurements were conducted around the lake. These measurements were used to create a turbidity model based on the spectral ratio of 550-nm and 670-nm bands. This turbidity model is applied to convert the spectral values of the SMI images to turbidity values at Nephelometric turbidity units (NTU) [6].

The Diwata-2 SMI images taken at 550-nm and 670-nm bands were geolocated and pre-processed using pre-flight radiometric calibration parameters, and atmospheric correction methods.

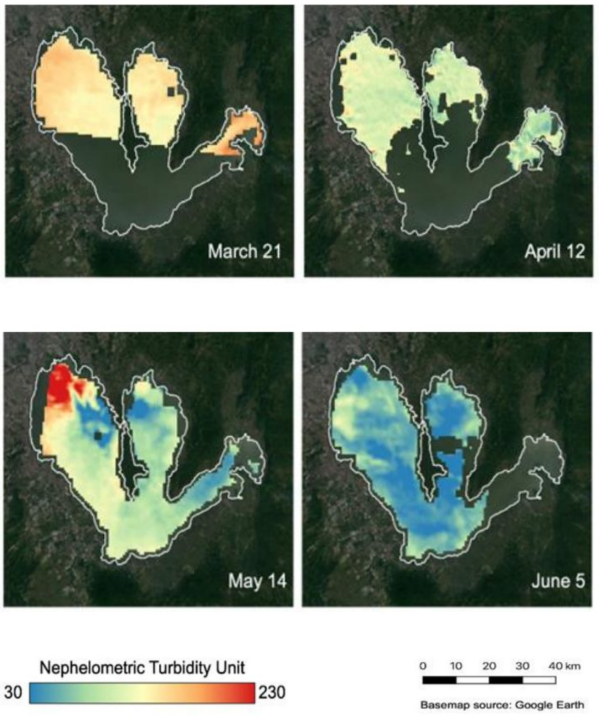

Figure 24: Turbidity Maps of Laguna Lake derived from Diwata-2 SMI Images from March 2019 to June 2019

For the 4-month observation period, a general decreasing turbidity trend was observed. Correlation analysis of wind speed and the observed turbidity suggests wind-induced resuspension of bottom sediments. Due to the increased spatial coverage and the consistent revisit period of Diwata-2, spatiotemporal monitoring of lake turbidity was demonstrated [6]. The processed observation data are shown in Figure 24.

On a natural disaster related application, Diwata-2 was used to assess and conduct a wide area projection of the ashfall coverage of the Taal volcano eruption in the Philippines last January 12, 2020. An archive image of

Diwata-2 of the area taken January 6, 2020, was used as the pre-eruption data reference. A post-eruption image for ashfall assessment of the same area was taken by Diwata-2 on January 27, 2020. The analyzed ashfall projection map of the area is shown in Figure 25.

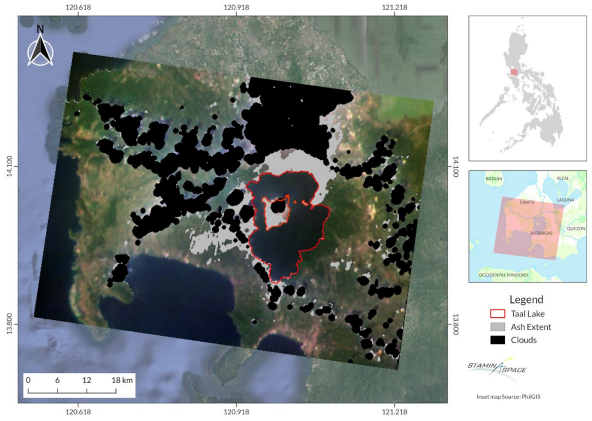

Figure 25: Taal Eruption Ashfall Projection using SMI Image

LESSONS LEARNED DURING DEVELOPMENT AND FROM OPERATIONS

Structure Simulation to Reduce Number of Vibration Tests

The satellite development team devoted more time to detail a structural model used for the analysis of Diwata-2 compared to Diwata-1. During Diwata-1 development, finite-element analysis (FEM) was only done using planar sheet elements to represent the panels. Meanwhile, representative values on these sheets were used to represent the rigidity effects brought about by the isogrid patterns on the panels. This method led to a 20 Hz difference in the normal mode frequency of the simulation to the actual results obtained from the actual vibration test. This disparity is large considering that a requirement of the primary normal mode to be above 50 Hz must be met, and hence a simulation result within 20 Hz of that limit must be verified with actual vibration tests.

Given this, the team decided to improve the model used for Diwata-2's structure simulation model. Instead of using a custom planar sheet to represent panels with isogrid patterns, actual 3D models from CAD were imported to the FEA software and processed accordingly to allow proper hexahedral meshing. The team also improved on the "bond" points in between panels to more accurately the bolted connection in between two surfaces. In Diwata-1, the default "glued" connection was used on the entire planar sheet edge and this possibly contributed to a less accurate result. For Diwata-2, as an upgrade, a "contact" type connection was used between adjacent mesh elements that most closely resemble the position of bolts. Moreover, the engineers incorporated a more accurate bolt connection representation from the calculated effective clamping force of the bolts.

These improvements increased the accuracy of the structure simulation to within +/- 5 Hz for the first two modes compared with the actual results. This result validated the improved accuracy from the additional measures that were observed in the structure model. This simulation approach could be helpful in future satellite development projects, especially those with limited access to test facilities, to reduce the number of actual tests.

Trade-offs in the Power Subsystem Upgrade

Diwata-2 inherited it's predecessor's core power subsystem, specifically the battery and PCU. However, unlike Diwata-1, this newer satellite contains more components and therefore, demands more power. This motivated the team to increase the power generation capacity of the satellite by adding more solar cells, especially in the new DSAP component.

While this solution may seem straightforward, the implementation and evaluation is not as simple. First, the design of a deployable solar paddle took significant engineering effort and testing resources. The development of the DSAP posed two major design challenges: structural integrity and thermal stability.

The structure integrity issue during vibration was solved by developing a new hinge mechanism that keeps the paddles at a stowed position as its default configuration. Upon user command, however, a burning mechanism cuts the string holding down the paddles and gently places it on an orthogonal configuration from its original state. It is also the responsibility of the hinge mechanism to keep this new position permanent. Multiple vibration and long-term stowing tests were performed to ensure that the hinge mechanism will not let the paddles deploy unintentionally.

Meanwhile, the thermal stability was solved by using a combination of carbon fiber-reinforced plastic (CFRP) and aluminum sheets pasted together acting as one rigid panel. The CFRP, in direct contact with the cells, serves as an insulator and effectively isolates the satellite body

from the heat produced by the solar cells during power generation in the sunlit phase.

The addition of the DSAP also caused the PCU to be modified to work with lower solar cell voltage due to high temperatures. This condition could cause the PCU to allow battery charging to continue even though it is already charged, especially in sudden high-power demand and low-power supply conditions (e.g. solar paddle is hot but is not pointing directly towards the sun). The PCU was also modified to accommodate higher current draw especially in hot conditions where the rated cut-off current of the positive thermal coefficient (PTC) fuse significantly decreases.

In summary, a seemingly small change of adding load components and the identified solution of increasing the power generation capacity by adding a solar paddle had a significant effect on the development time and evaluation through testing. More importantly, modifications such as these should be subjected to a more thorough design review before entering more advanced stages in satellite development to prevent unexpected bottlenecks.

In the future, the satellite developers plan to continue improving the power subsystem design by exploring battery cells with higher power density and by considering more structurally and thermally stable configurations. With the lessons learned from the development of Diwata-2, these future designs will be subjected to much stricter design review and subsystem-level testing before proceeding with further system integration.

Modification of Satellite Maneuver Procedure based on Observed Performance

Since the launch of Diwata-2, continuous evaluation and analysis of the flight data for performance improvement were conducted. With the heritage satellites Diwata-1, RISING-2, and RISESAT, flight data analysis yielded methodologies to improve the performance of ADCS [13][14]. Additionally, for the in-orbit Diwata-2, the satellite operators also adapted operational maneuvers based on the performance of the attitude sensor elements to improve the quality of satellite observation. Conventional observation begins with the coarse attitude determination (i.e. SAS and GAS) before shifting to fine attitude determination (i.e. STT). This approach, however, occasionally produced unsatisfactory results with Diwata microsatellites. Stray light towards the sensing elements have proven to be detrimental to the estimation accuracy of both the coarse and fine attitude determination systems. SAS and STT are especially sensitive to albedo: SAS returns an inaccurate sun vector while STT fails to sample recognizable star patterns with a relatively high brightness. This situation often led to observation accuracy of around ±50 km from the intended target. With the HPT optical payload's narrowest field-of-view at 2.2 km, this accuracy is insufficient.

As a solution, the satellite operators began to use STT at the eclipse phase of the orbit where it could produce an accurate attitude based on clearly distinguishable star patterns. Before entering the sunlight phase, attitude determination mode is shifted to FOG integration. In this mode, the last accurate attitude measurement by the STT is integrated based on the gyroscope rates until the moment of capture. This technique eliminates the effect of external noise on the observation leaving only a possible detriment of gyroscope drift on the calculation. However, for relatively short operations, this effect is minimal as confirmed by much-improved observations from using this technique.

This observation method, when supplemented with the calibration of alignment matrices, yields improved results with an average accuracy of ±5 km and a best performance of ±2 km that sits within the FOV of the HPT.

Acknowledgments

The development of the Diwata-2 microsatellite was made possible by the collaboration of the Philippine's PHL-Microsat program, University of the Philippines - Diliman, Japan's Tohoku University, and Hokkaido University. Limited radiation testing of experimental modules was conducted in partnership with the Philippine Nuclear Research Institute. The team would also like to acknowledge the support given by the Japan Aerospace Exploration Agency (JAXA) during the compliance and acceptance procedures, and for the successful HII-A launch and release of its payloads into space. The PHL-Microsat project, and the subsequent STAMINA4Space program, was funded by the Philippine government under the state's Department of Science and Technology (DOST), Philippine Council for Industry, Energy, and Emerging Technology Research and Development (PCIEERD).

References

1. Radtke, K., Mann, H., Weller, D., Kirch, L., and Prütz, R., "The World Risk Index 2018", World Risk Report 2018, Berlin: Bündnis Entwicklung Hilft, November 19, 2018.

2. Padagdag, J.M., “The Philippine Disaster Risk Reduction Management System”, ADRC Visiting Researcher Program 2018B, Accessed: *https://www.adrc.asia/countryreport/PHL/2018/Philippines_CR2018B.pdf*

3. UNDRR and ADPC, “Disaster Risk Reduction in the Philippines: Status Report 2019, Accessed: *https://www.unisdr.org/files/68265_682308philippinesdrmstatusreport.pdf*

4. Jha, S., A. Martinez, P. Quising, Z. Ardaniel, and L. Wang, “Natural Disasters, Public Spending, and Creative Destruction: A Case Study of the Philippines”, ADBI Working Paper 817, Tokyo: Asian Development Bank Institute, 2018. Accessed: *https://www.adb.org/publications/natural-disasters-public-spending-and-creative-destruction-philippines*

5. Asada, S., Abe, N., Andoh, K., & Fleeter, R., “Launching Small Satellites on the H-IIA Rocket”, 17th Annual AIAA/USU Conference on Small Satellites, Paper SSC-03-II-4, 2003.

6. Perez, G.J., Felix, M.J., Namuco, S., Felicio, F., Merida, H., Vergel, K.K., Castro, E., and Marciano Jr., J.J.S., “Environmental Monitoring Using Philippines’ Diwata-2: A Case Study in Laguna de Bay”, 40th Asian Conference on Remote Sensing (ACRS 2019): Progress of Remote Sensing Technology for Smart Future, Vol.1, P. 1177-1182, October 14-18, 2019.

7. Takahashi, Y., Kurihara, J., and Fukuhara, T., “Advanced remote-sensing sensors for micro-satellite and their application,” IEICE Technical Report, SANE2011-69, 2011.

8. Sakamoto, Y., Sugimura, N., Fukuda, K., Kuwahara, T., Yoshida, K., Kurihara, J., Fukuhara, T., and Takahashi, Y., “Development and Flight Results of Microsatellite Bus System for RISING-2,” Transactions of the Japan Society for Aeronautical and Space Sciences, Aerospace Technology Japan, Volume 14 Issue ists30, P. 89-96, 2016.

9. Sakamoto, Y., Gonzalez, A., Labrador, J.L., Guba, G., Paler, H.B., Kuwahara, T., Yoshida, K., Ishida, T., Kurihara, J., and Takahashi, Y., “Development and Flight Operations of Microsatellite Bus System for Diwata-1,” International Symposium on Space Technology and Science, Matsuyama, Japan, 2017-f-089, 2017.

10. Kurihara, J., Takahashi, Y., Sakamoto, Y., Kuwahara, T., and Yoshida, K., “HPT: A High Spatial Resolution Multispectral Sensor for Microsatellite Remote Sensing,” Sensors, 18-619, February 2018.

11. Salvatus, J., Constante, M.A., Violan, E.P., Salces, A., Paet, L.B., Talampas, M.C., and Marciano, J.J., “Development of Deployable Antennas for the Diwata-2 microsatellite’s amateur radio payload,” IEEE International Conference on Communication, Networks and Satellite, Semarang, Indonesia, 2017.

12. Fujita, S., Sato, Y., Kuwahara, T., Sakamoto, Y., and Yoshida, K., “On-ground Verification of Attitude Control System for 50-kg class Microsatellite using a Hardware-in-the-loop Simulator,” 68th International Astronautical Congress (IAC), IAC-17-B4.6A.11, Adelaide, Australia, September 2017.

13. Fujita, S., Sato, Y., Kuwahara, T., Sakamoto, Y., and Yoshida, K., “Development and Ground Evaluation of Ground-Target Tracking Control of Microsatellite RISESAT,” Transactions of the Japan Society for Aeronautical and Space Sciences, Aerospace Technology Japan, Volume 17 Issue 2, P. 120-126, 2019.

14. Sato, Y., Kuwahara, T., Sakamoto, Y., and Yoshida, K., “Development and Ground Evaluation of Fast Tracking Algorithm for Star Trackers,” Transactions of the Japan Society for Aeronautical and Space Sciences, Aerospace Technology Japan, Volume 16 Issue 3, P. 202-209, 2018.

15. Fujita, S., Sato, Y., Kuwahara, T., Sakamoto, Y., and Yoshida, K., “Attitude Maneuvering Sequence Design of High-Precision Ground Target Tracking Control for Multispectral Earth Observations”, IEEE/SICE International Symposium on System Integration (SII), 2019.

16. Kuwahara, T., Fukuda, K., Sugimura, N., Hashimoto, T., Sakamoto, Y., and Yoshida, K., “Low-cost Simulation and Verification Environment for Micro-satellites,” Transactions of the Japan Society for Aeronautical and Space Sciences, Aerospace Technology Japan, Volume 14 Issue ists30, P. 83-88, 2016.

17. Sato, Y., Fujita, S., Kuwahara, T., Katagiri, H., Sakamoto, Y., and Yoshida, K., “Improvement and verification of satellite dynamics simulator based on flight data analysis,” IEEE/SICE International Symposium on System Integration (SII), 2017.